

Solid Solution Strengthening in High-Entropy Alloys

Ibrahim Ondicho, Benard Alunda and Kahinga Kamau

Abstract

This book chapter discusses solid solution strengthening (SSS) as one of the main hardening mechanisms in high-entropy alloys (HEAs) that form basis as one of its core effects (lattice distortion). The various techniques used to quantify SSS and the role of different substitutional and interstitial elements/atoms in improving the strength of HEAs are outlined in detail. This review provides a good assessment on ways to enhance the mechanical properties of HEAs to suit the extreme demands of modern engineering applications. Based on theoretical modeling and experimental validation, Al and Nb provide superior substitutional SSS in face-centered cubic and body-centered cubic crystal structures, while carbon has a 50% more effect on improving the mechanical properties of HEAs than in stainless and twinning-induced plasticity steels. Moreover, a detailed description of the application of machine learning in design of HEAs shows that trial and error can be eliminated in identifying HEAs with exceptional yield strength. The atomic size difference should be used to evaluate the lattice distortion effect.

Keywords: high-entropy alloys, solid solution strengthening, lattice distortion, interstitials

1. Introduction

For decades since the Iron Age, many engineering applications have relied upon metallic materials that are designed on the basis of one principal element. Their physical properties of the matrix are enhanced by introducing small quantities of alloying elements. However, with the increment of complex engineering systems operating in extreme conditions, the need for materials with excellent mechanical properties has also increased exponentially. For instance, even though austenitic stainless steels have been successfully used as a structural material in a nuclear reactor core, irradiation embrittlement, irradiation-induced stress corrosion cracking and low fatigue life limits their extensive application in design of future nuclear reactors [1]. The aforementioned challenges among others require new materials that withstand the physical demands of their application environments that cannot be harnessed from the current traditional alloys. Recently, a new alloy design approach, which utilizes more principal elements in a metallic alloy was proposed by Yeh et al. [2, 3] and Cantor et al. [4]. These alloys, which were christened as high-entropy alloys (HEAs), consist of five or more principal elements with a concentration range of 5–35 at.

%. These alloys have been reported to possess some excellent physical and mechanical properties compared to the conventional alloys [5–7]. This makes them suitable candidates for structural applications such as chemical and nuclear reactors, which have highly corrosive and extreme temperatures, aircraft engine turbines, hydrogen storage facilities, where creep strength and resistance to hydrogen embrittlement are key design considerations [8–11].

It is noteworthy that the strengthening mechanisms in HEAs are not any different from the ones observed in conventional alloys although the activation pathways and their contribution to strengthening can be different. These strengthening mechanisms include solid solution strengthening (SSS), grain boundary (GB) strengthening, dislocation strengthening (DS), precipitation hardening (PH), transformation-induced plasticity (TRIP), twinning-induced plasticity (TWIP), and composite microstructures (CM) [12–19]. Among these strengthening mechanisms, SSS is the only inherent hardening mechanism courtesy of the high atomic size mismatch in the crystal structure inducing lattice distortion, which is enlisted as one of the core effects of HEAs. Consequently, SSS forms the basis upon which other strengthening mechanisms are built on, hence, warranting in-depth review on the recent advances as new HEAs are designed. Therefore, this chapter discusses the SSS mechanism in HEAs spanning from the theoretical and analytical method to experimental techniques used in screening of this hardening mechanism.

2. Solid solution strengthening mechanism in high-entropy alloys

In conventional alloys, solid solution strengthening can be achieved by substitution or interstitial atoms of alloying elements (**Figure 1**). In the former, solute atoms replace solvent atoms in the crystal structure while in the latter, the smaller interstitial atoms such as carbon, nitrogen and boron, tend to dissolve into the interstitial spaces within the atoms of the solvent element. Both substitutional and interstitial SS strengthening induces a local lattice distortion as shown in **Figure 2a**. The stress fields caused by both substitutional and interstitial atoms coupled with the local lattice distortion impede dislocation motion and make it difficult for the introduction of new dislocations into the crystal structure during plastic deformation. Therefore, it requires higher stresses to introduce and induce dislocation motion past the strain fields and the solvent atoms. It is important to note that lattice distortion is localized in

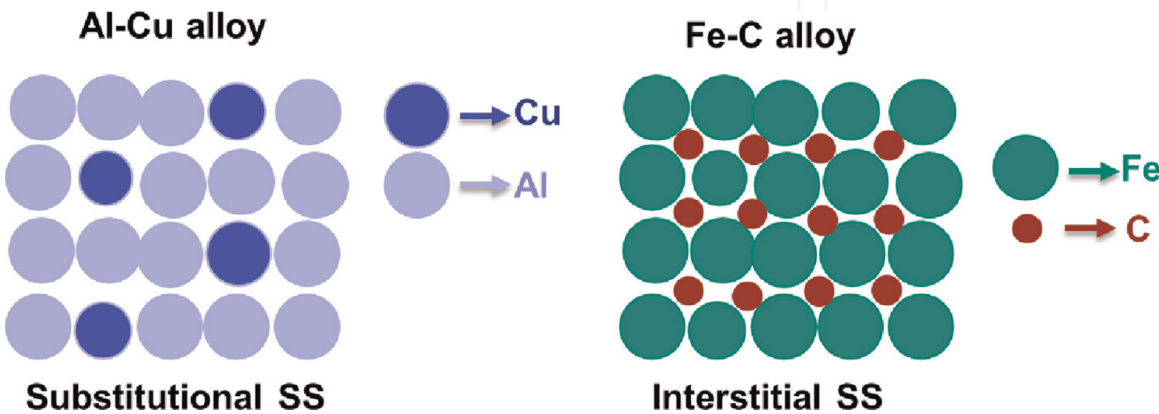


Figure 1.
Schematic drawing of substitutional and interstitial solid solution strengthening in conventional alloys.

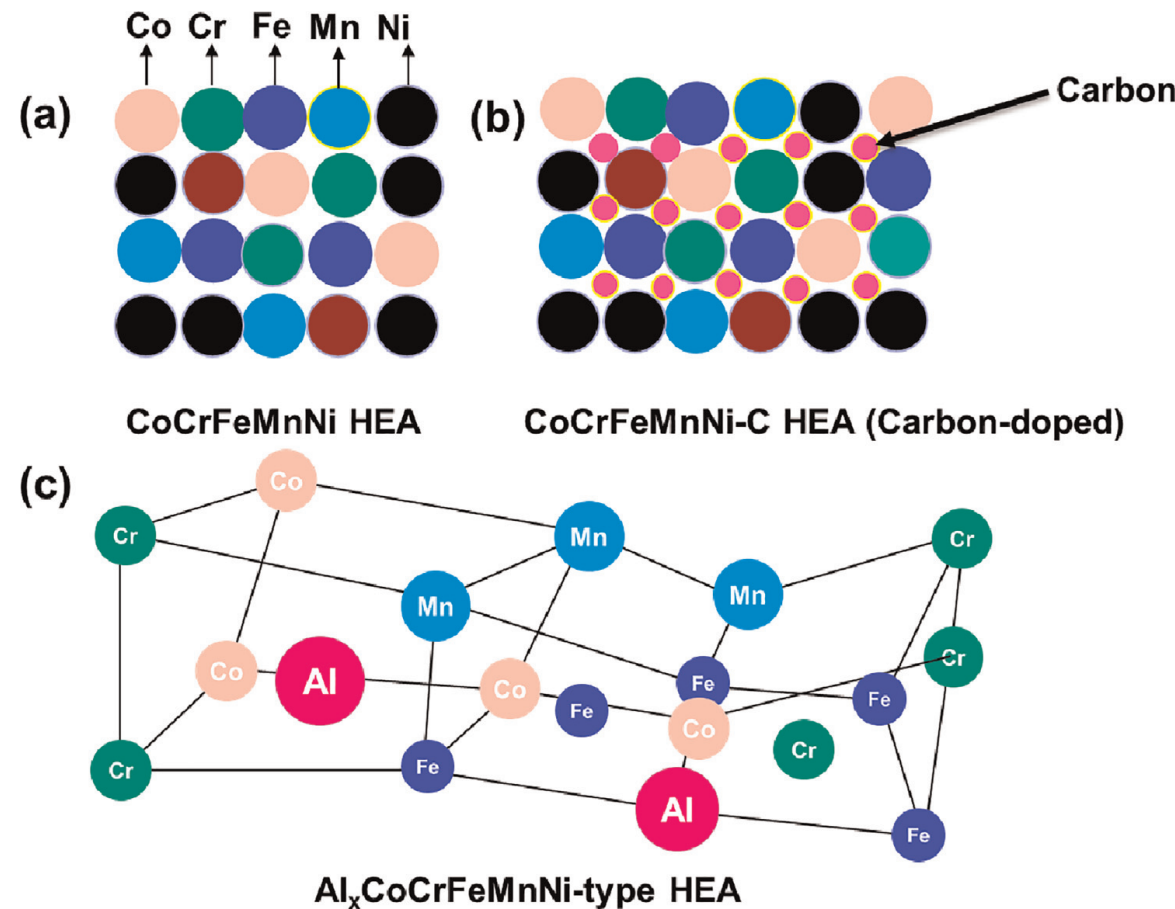


Figure 2.
Schematic diagram of (a) CoCrFeMnNi equiatomic high-entropy alloy crystal structure (b) carbon-doped CoCrFeMnNi high entropy alloy, and (c) severely distorted crystal structure of a typical Al_xCoCrFeMnNi high-entropy alloy.

conventional alloys as compared to global distorted crystal lattice in HEAs as shown in **Figure 2b**.

2.1 Estimating solid solution strengthening in high-entropy alloys

2.1.1 Theoretical models

Labusch et al. [20] developed a model that describes the SS hardening in conventional multicomponent alloys by considering the impact of frictional effect caused by the continuous interaction of the solute and solvent atoms on the dislocation motion as in the Fleischer model [21]. According to this model, the effect of solute atoms acting as blocking barriers is negligible compared to the frictional effect. The Labusch model ascribes SS hardening of an alloy to its elastic mismatch and atomic size misfit [22].

$$\Delta \sigma_{ss} = B_i X_i^{\frac{2}{3}} \quad (1)$$

where the parameters B_i and ϵ_i can be expressed as:

$$B_i = 3\mu\epsilon_i^{\frac{4}{3}}Z; \quad \epsilon_i = \left(n_i'^2 + \alpha^2\delta_i^2\right)^{\frac{1}{2}} \quad (2)$$

where X_i is the solute content and B_i is a constant that depends on the alloy shear modulus, mismatch parameter and a fitting constant Z as shown in Eq. (2): The mismatch parameter is a convolution of the elastic misfit and the atomic size misfit, which can be described by Eq. (3):

$$n'_i = \frac{n_i}{1 + 0.5|n_i|}; \quad n_i = \frac{d\mu}{dX_i} \frac{1}{\mu}; \quad \delta_i = \frac{da}{dX_i} \frac{1}{a} \quad (3)$$

where a is the lattice parameter and α being the parameter that accounts for difference in interacting forces between edge and screw dislocations. For the screw dislocations the acceptable value is $3 < \alpha < 16$ while for the edge dislocations $\alpha > 16$.

The lack of a reference atom in HEAs, especially in equiatomic or near equiatomic alloys, complicates the direct application of the Labusch model in evaluating SS hardening in HEAs. Therefore, Toda-Caraballo et al. proposed another theoretical model based on the Gypen and Deruyttere's model [23] to calculate SS hardening in HEA by taking into account the average interatomic distance S_{ij} and average lattice constant:

$$S_{ij} = \frac{S_{ii}^2 K_i X_i + S_{jj}^2 K_j X_j}{S_{ii} K_i X_i + S_{jj} K_j X_j} \quad (4)$$

where s_{ii} is the atomic size of pure elements, K_i is the bulk modulus of pure elements and x_i is the concentration of the elements. The average lattice constant of the alloy, a , is calculated as:

$$a = f \sum_{ij} S_{ij} X_i X_j \quad (5)$$

where f is a constant depending on the crystal structure assuming a rigid sphere model (e.g., $f = p/2$ for FCC).

The above approach was adopted for HEAs due to their unique design in which five or more principal elements are involved in equiatomic or close to equiatomic compositions. Therefore, it is difficult to distinguish between the solvent and solute atoms since there is no reference atom and the entire crystal lattice is severely distorted as shown in **Figure 2b**. As a result, the Labusch model cannot be directly implemented in HEAs since it becomes difficult to determine the average lattice parameter theoretically. Toda-Caraballo compared predicted and experimental lattice parameters and an overestimation in bcc HEAs and underestimation in fcc HEAs was observed. A corrective multiplicative factor A was included and Eq. (3) can be re-written as:

$$a^{ave} = s_p^{ave} f_p A \quad (6)$$

where $A = 0.98$ for bcc and $A = 1.01$ for fcc HEAs. The other parameters remained the same as expressed in the Labusch model [22]. Furthermore, the calculated misfit of CrFeNbV equiatomic HEA shows that the model can be used to track the change in the interatomic spacing. It was found that this change obeys a linear relationship and can easily be regarded as an extension of the Vegard's law. The effect of different elements on the SS hardening of HEAs was mapped out by evaluating the average interatomic spacing as their atomic concentration is varied. For instance, both theoretically and experimentally, it was established that addition of Cr enhances the strength of CoFeNi by increasing its interatomic spacing while addition of Fe softens CoCrNi [22]. Okamoto

et al. used root-mean-square atomic displacements X-ray diffraction (XRD) and first-principles calculation to predict the strength of the equiatomic CoCrFeMnNi HEA, which can scaled to its MEA subsets (i.e CrMnCoNi, CoCrNi, FeCoNi, MnFeCoNi, MnCoNi, MnFeNi, and CrFeCoNi). It was established that the MSAD increases as the atomic number of pure elements decreases. Moreover, the lattice distortion depends on both the atomic size of the pure element and the surrounding atom in HEAs. For instance, Mn has a MSAD of 60.9 pm² in CrMnFeNi quaternary alloy compared to 26.2 pm² in MnFeCoNi HEA. Therefore, the choice of elements has a great influence in lattice distortion of HEAs [24]. Moon et al. [25] utilized a geometrical model to evaluate SSS in a single crystal of CoCrFeMnNi HEA based on the intrinsic residual strain criterion proposed by Ye et al. [26] in conjunction with lattice friction stress. It was empirically established that there is an exponential increase of the normalized intrinsic yield strength (σ_o/E) with an increasing residual mean strain (RMS) and Eq. (7):

$$\frac{\sigma_o}{E} = Y_o + A \cdot \exp \left(B \cdot \sqrt{\langle \varepsilon^2 \rangle} \right) \quad (7)$$

where ε^2 is the RMS and Y_o , A, and B are fitting parameters. The values of aforementioned parameters were found to be 27.81, 35.57, and 202.28, respectively, using a minimization function of experimental and calculated yield stress values, $f = \sigma_{\text{experimental}} - \sigma_{\text{calculated}} \rightarrow \min$ [25]. The comparison of the experimental and calculated data is shown in **Figure 3b**.

Ultimately, it was elucidated that there was an exponential increment of the intrinsic yield strength (i.e. lattice friction) with an increasing residual strain. In addition, the CoCrFeMnNi, which has a higher RMS residual strain than the quaternary CoCrFeNi HEA, was reported to have a 14.3% higher in intrinsic yield strength. This enhanced solid solution strengthening was ascribed to the presence of Mn atoms, which tend to enhance mean-square atomic displacements (MSADs) as confirmed theoretically and experimentally by Okamoto et al. [24].

2.1.2 Machine learning

Machine learning (ML) is a subset of involves using computer algorithms to study the available data and statistics and ultimately improving the performance or the output of the systems. ML has been successfully used to accurately predict phase stability in HEAs [31–33]. Recently, Wen et al. [34] recently demonstrated that ML is able to identify the underlying factors that contribute to SSS. It was established that the electronegativity difference between local interacting atoms plays a dominant role in SSS of HEAs by inducing variation of the atomic level pressure or stresses, which determines the bonding strength of element. The superior SSS in HEAs is ascribed to the greater driving force that is required to induce an electronic rearrangement [35]. Therefore, the authors proposed a model based on the electronegativity difference in predicting HEAs with superior SSS.

$$\Delta \sigma = \xi \cdot Z \cdot G \cdot \delta X r \dots\dots\dots (8)$$

Based on this model, it was established that Mn and Cu had no profound influence on the SSS when added in a CoCrFeNi matrix while refractory elements such as Hf, Zr, Nb, and Mo showed a remarkable contribution to the SSS effect in both CoCrFeNi

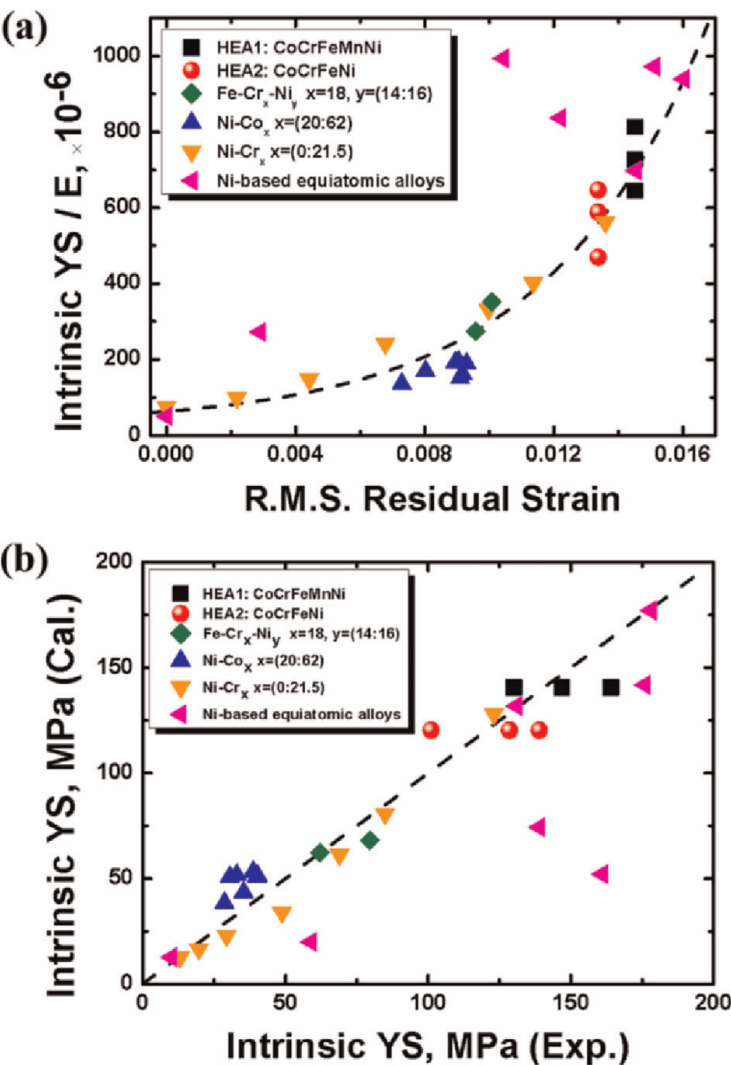


Figure 3.
(a) Relationship between intrinsic yield strength (YS) normalized by the elastic modulus and the RMS residual strain for low to high entropy alloys and (b) comparison of the calculated and experimental data. Adopted from Moon et al. [25]. The other experimental data was referenced from [27, 28, 29, 30].

and CoMnFeNi base matrix. It was further elucidated that a higher Co and Cr content with a decreased amount of Mn enhances SSS, which is consistent with the observations made by Toda Caraballo [22].

Huang et al. [36] also utilized ML to model SSS in HEA using atomic environment and interactions as the input parameters. The developed ML model was used to predict hardness of single solid solution HEAs by combining the critical theoretical SSS descriptors such as shear modulus, atomic size mismatch, bulk modulus and phase stability descriptors such as mixing enthalpy, mixing entropy, and a phase stability descriptor, Pauling electronegativities, valence electron concentration (VEC) and melting temperature. In this study, Random Forest (RF) was selected as the best algorithm for hardness prediction over the other four commonly used algorithms (Multilayer Perceptron, LibSVM, Bagging, and k-Nearest Neighbor). RF was adopted based on its high correlation coefficients (CC), low mean absolute error (MAE) and root mean squared error (RMSE).

Previously, Ding et al. [37] proposed that competition between lattice strains and concentration differences give rise to a strong local concentration fluctuations in CrFeCoNiPd HEA, which induces a strong resistance to dislocation glide. Based on the

local chemical environment, Huang et al. [36] proposed a modified physical model for SSS by adding the charge transfer (dQ) between atoms to the Varvenne and Maresca-Curtin models. This charge transfer induces atomic-level pressure (DP_{solute}) fluctuations, which dominates the SSS of several Cantor based HEAs [35]. According to the Varvenne model, the yield strength and atomic-level pressures have the following relationship $\sigma_{\text{SSS}} \propto \Delta P_{\text{solute}}^{4/3}$ and the first ionization energy (E_I^{1st}) is used to estimate the charge transfer. Based on the aforementioned parameters, the following equation was proposed to quantify the correlation between dQ factor and σ_{SSS} .

$$\begin{aligned}\sigma_{\text{SSS}} &= M \times 0.051\alpha^{-1/3}G \left(\frac{1+\nu}{1-\nu} \right)^{4/3} f_1(\omega_c) \times m_o (E_I^{1st})^{-4/3} \\ &= m_v \times m_o (E_I^{1st})^{-4/3}\end{aligned}\tag{9}$$

where M denotes the Taylor factor, α and ν are line tension parameter and Poisson's ratio, respectively, G is the shear modulus, $f_1(\omega_c)$ is the minimized core coefficient, m_o is the transfer coefficient between dQ and σ_{SSS} and all the material constants are merged and termed as m_v . the results of fitting as shown in **Figure 4a**, indicate that σ_{SSS} has a linear relationship with the dQ factor. A total of 556 as-cast alloys were screened using the developed ML-SSS model for single phase solid solution (FCC/BCC) and hardness prediction in HEA compositional space [36]. Two HEA families CrMoNbTi and FeNiCuCo with a dominant BCC- and FCC-single phase solid solution, were adopted for alloy design and experimental validation with a compositional variation of between 5 and 35% of each element. Interestingly, the predicted and experimental hardness of SPSS-HEAs from the five equiatomic and non-equiatomic exhibited an excellent agreement as shown in **Figure 4b** and **c** for FeNiCuCo (FCC) and CrMoNbTi (BCC) HEAs, respectively. Moreover, in this study it was demonstrated that some non-equiatomic HEAs (FCC or BCC) have superior hardness compared to their equiatomic counterparts. For instance, Fe₃₂Ni₁₂Cu₂₇Co₂₉ HEA has a 236 HV while Fe₂₅Ni₂₅Cu₂₅Co₂₅ HEA has 184 HV for the FCC family and Cr₁₈Mo₃₂Nb₃₅Ti₁₅ has 607 HV while Cr₂₅Mo₂₅Nb₂₅Ti₂₅ has hardness value of 558 HV for the BCC family based on the experimental results. Therefore, this shows that the developed ML-SSS model is able to accurately screen a large compositional space of HEAs and identify alloys with superior mechanical properties.

2.1.3 Experimental techniques

XRD and Hall-Petch relationship are some of the experimental techniques that have been used to experimentally mapping out SSS in HEAs [38–40]. In XRD, the

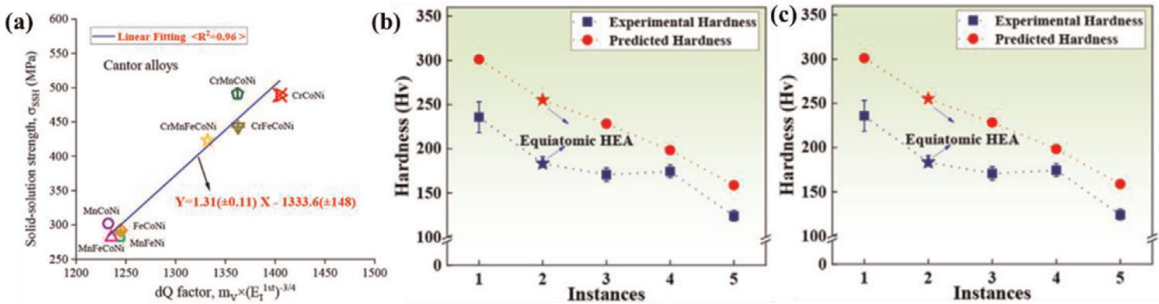


Figure 4.
(a) Charge transfer part versus experimentally measured solid solution strengths s_{SSS} of cantor alloys. The predicted and experimental hardness of (b) FeNiCuCo and (c) CrMoNbTi high entropy alloys.

change in lattice constant due to the large atomic size misfit experienced in HEAs as a result of having more principal elements with different atomic sizes has been observed in many HEA systems. Macro- or micro-chemical inhomogeneity can lead to a change in lattice parameter in HEAs, which causes a proportional change of 2θ in XRD diffractograms according to the classical Bragg's law ($n\lambda = 2d\sin\theta$). From the Bragg's law, an obvious indication of SSS is the shift of peaks to lower 2θ angles in HEA possessing high degree of SS hardening compared to the reference alloy [41]. This is due to the change in the average lattice parameter of HEAs caused by high atomic size misfit [42]. Addition of Al either as a principal or as alloying element has been used to induce substantial lattice distortion in HEAs systems due to its large atomic size [43]. Wang et al. [43] studied the effect of Al addition in the crystal structure evolution of $\text{Al}_x\text{CoCrFeNi}$ HEA system and established that fcc solution is formed when <11 at.% of Al is used while bcc is stabilized when Al content is >18.4 at.%. A careful observation of XRD peaks $(200)_{fcc}$ and $(200)_{bcc}$ for $\text{Al}_0 - \text{Al}_7$ and $\text{Al}_{0.7} - \text{Al}_{2.0}$ respectively, shows a peak shift to lower 2θ angles with increasing Al content due to the expansion of the d-spacing of both fcc and bcc phases as shown in **Figure 5a** and **b**. A proportional increase of the lattice constant values for both fcc and bcc values is observed as Al content is increased as shown in **Figure 5c**. Changes in the lattice constant and Vickers hardness exhibit different behaviors. Addition of $\text{Al}_{0.1}$ to the base system (CoCrFeNi) induces substantial change in lattice constant while a gradual increase is observed between $\text{Al}_{0.2} - \text{Al}_{0.5}$ in the fcc region. However, there is minimal change in hardness between $\text{Al}_0 - \text{Al}_{0.4}$ while a drastic change is observed in the alloy with $\text{Al}_{0.4}$ content, which is in the boundary of single-phase fcc and fcc + bcc regions. Therefore, this infers that substantial SSS is achieved when the Al content is above $x = 0.5$ (11 at.%). $\text{Al}_{0.9}$ alloy (bcc) has the highest hardness value of all the alloys with a bcc phase although it has the least lattice constant. $\text{Al}_{2.0}$ alloy has the highest lattice constant. Chen et al. [44] observed a similar shift of peaks with the addition of different amounts of Nb and Cr to the base of MoCrTiAl bcc HEA as shown in **Figure 6**. Addition of Nb to MoCrTiAl as shown in **Figure 6b** and **c**, induces a slight peak shift to lower 2θ angles signifying a proportional expansion of d-spacing and eventual increase of the lattice constant. It is interesting to note that replacing Cr with Nb induces a larger peak shift to lower 2θ angles than when Nb content is less. Therefore, it is reasonable to deduce that Nb has a superior SSS ability compared to Cr in both fcc- and bcc-based HEAs [22, 44]. However, Cr was reported to be a superior SSS element in CoFeNi fcc compared to Co, Fe, Ni elements [45]. Moreover, the sensitivity of change in lattice spacing in higher 2θ values can be observed in **Figure 4**, where peak shift is higher compared to that at lower 2θ values. It is important for the readers to examine carefully the accuracy of lattice parameter values reported in literature when describing SSS behavior of HEAs even though the trend may remain unchanged in some cases. The authors [43, 44] have used an extrapolation function $\frac{1}{2}(\cot^2 \theta + \cot \theta \cdot \cos \theta)$ according to Nelson-Riley [46], to calculate accurate lattice parameter values, which are extrapolated back to $\theta = 90^\circ$, where inherent systematic errors of diffractometers are minimized instead of using single peak such as ref. [45] or all peaks without extracting systematic errors [47].

The yield strength (YS) of metals and alloys is related to grain size by the classical Hall-Petch equation [48, 49]:

$$\sigma_y = \sigma_0 + \frac{K}{\sqrt{d}} \quad (10)$$

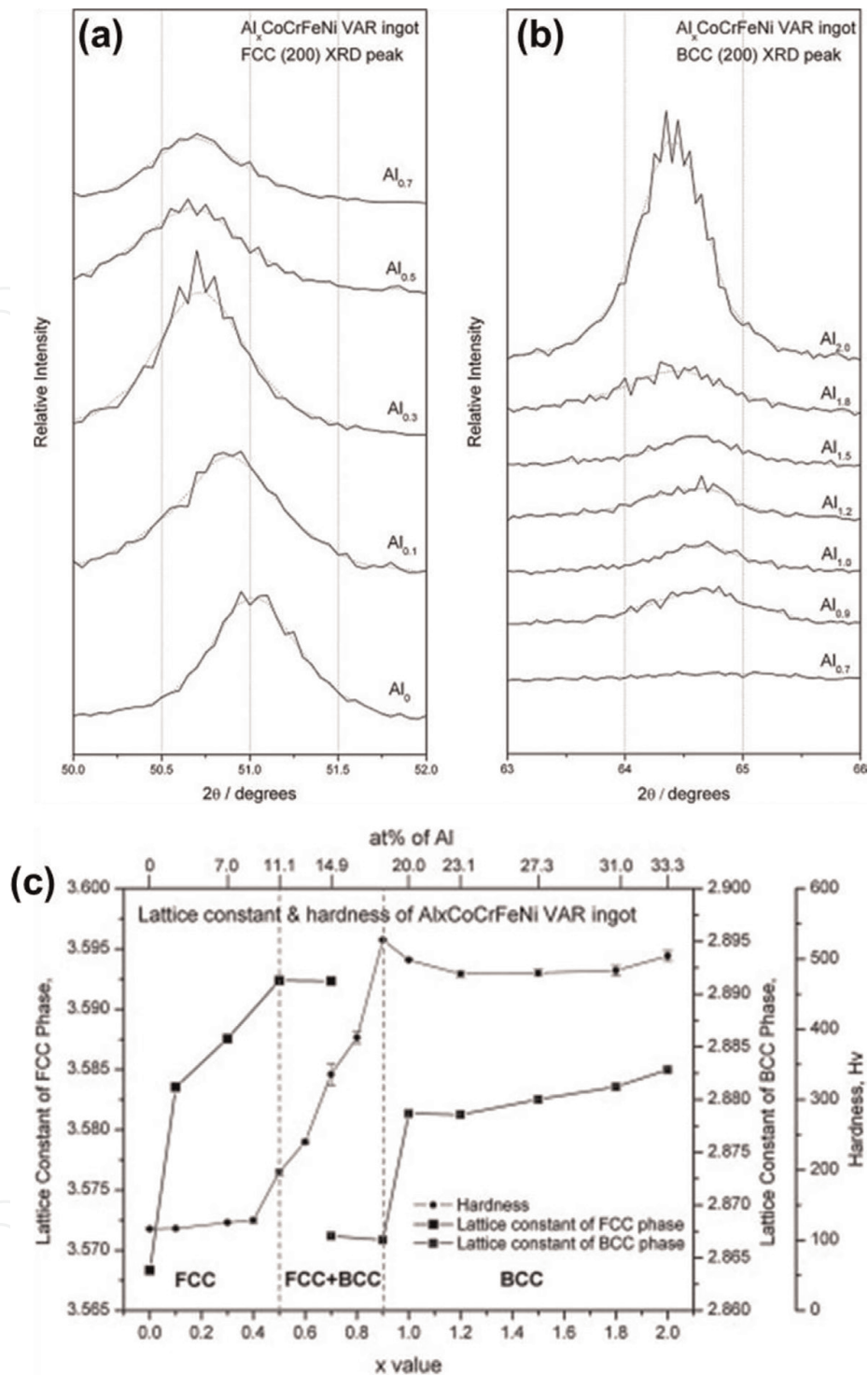


Figure 5. XRD patterns showing peak shift of 200 peaks of $\text{Al}_0 - \text{Al}_7$ and $\text{Al}_{0.7} - \text{Al}_{2.0}$ for (a) fcc and (b) bcc phases, respectively. (c) Lattice constant and hardness of the $\text{Al}_x\text{CoCrFeNi}$ alloys as functions of Al content. Symbol (\blacktriangle) and symbol (\blacksquare) denote lattice constants of FCC and BCC phases, respectively. Symbol (\bullet) denotes hardness. Adopted from reference [43].

where σ_y is the YS, σ_o is the friction stress (which is defined as the flow stress required to move dislocations within the grain matrix without the effect of grain boundaries), K is a constant, which depends on the ability of the grain boundaries to resist transmission of dislocations from one grain to the adjacent grain, and d is the mean grain size. To evaluate SSS, first term on the right-hand side of Eq. (4) (friction

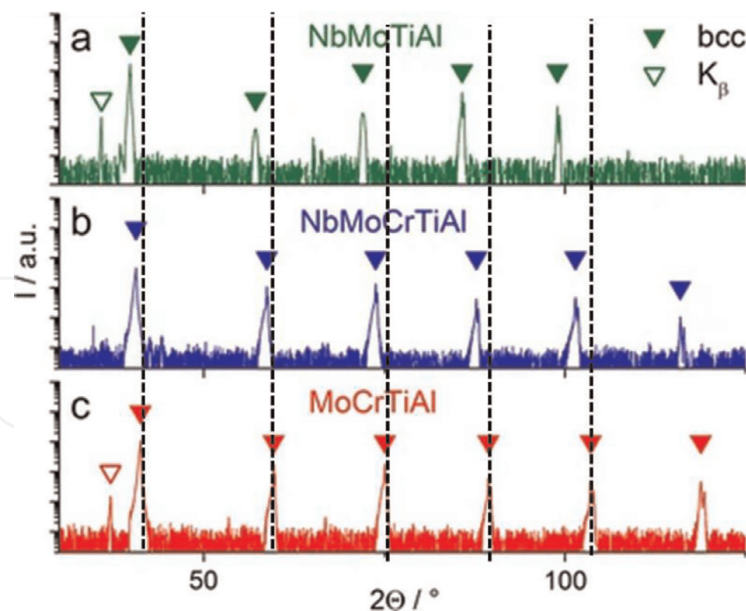


Figure 6. XRD patterns with logarithmic intensity scale of alloys with equiatomic composition in homogenized condition: (a) NbMoTiAl annealed at 1500°C, (b) NbMoCrTiAl annealed at 1300°C, and (c) MoCrTiAl annealed at 1200°C, each for 20 h. peaks arising from residual Cu-K β radiation are indicated by open triangles. The dotted lines are used to indicate peak shifts with the change of alloying elements (Nb and Cr). Data is adopted from ref. [44].

stress), will be considered. Friction stress is affected by solutes and any second phases present in the grain matrix. To effectively and accurately determine the effect of SSS on the mechanical properties of HEAs, the friction stress values of single-phase fcc alloys were compared as shown in **Figure 7**. Yoshida et al. [39] utilized the theoretical models of Toda-Caraballo et al. to predict SSS in HEAs with a single-phase fcc and compared the results with trends of their respective friction stress values obtained from the Hall-Petch equation. The theoretical model is used to predict the atomic size misfit HEA, where lattice distortion and eventual SSS is expected to be high in HEAs

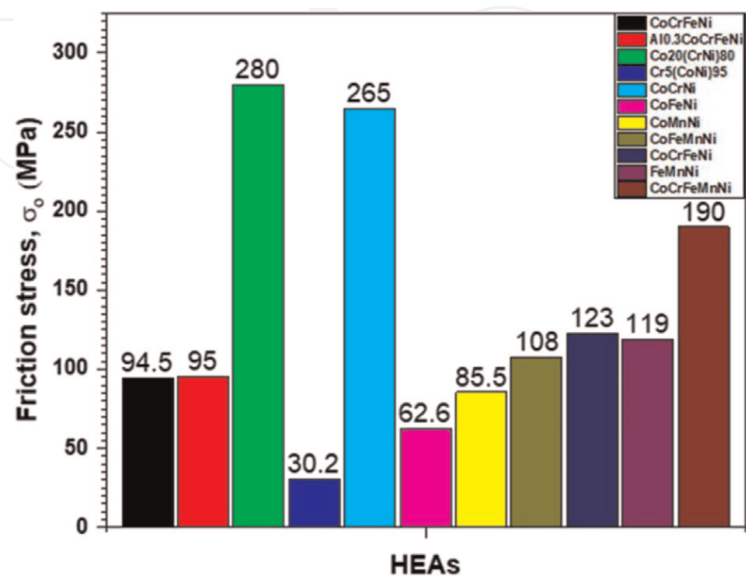


Figure 7. Friction stress of various HEAs with single-phase fcc obtained from the Hall-Petch relationship using tensile yield stress. Data extracted from Refs. [39, 40].

with large atomic size misfit especially in those alloys with Cr, Mn, Nb and Al as constituent elements [22, 39, 40, 43, 47]. Theoretically, it was established that $\text{Cr}_{20}(\text{CrNi})_{80}$ MEA has the largest atomic size misfit; hence, its crystal structure is severely distorted with a potential of having SSS as one of the main contributing mechanisms towards its overall YS. Further experimental investigation using the Hall-Petch equation, accurately validated the theoretical prediction by showing that indeed $\text{Cr}_{20}(\text{CrNi})_{80}$ MEA had the highest friction stress compared to other HEAs and MEAs under study. This is despite this alloy having a non-equiatomic composition and three constituent elements. Surprisingly, its friction stress (280 MPa) was even higher than that of CoCrNi MEA (265 MPa) previously reported by [40] and the quinary equiatomic CoCrFeMnNi HEA (194 MPa) [50] as shown in **Figure 7**. A recent study by Ondicho et al. [51] reported a continuous decrement of friction stress as the amount of Fe is increased in the equiatomic CoCrFeMnNi HEA as the other four elements remain in equiatomic composition. This increment of Fe weakens both SSS and GB strengthening because of monotonic decrease of friction stress and Hall-Petch coefficient. This phenomenon elucidates on the critical role the type and amount of constituent elements plays in SSS of HEAs. Therefore, simple stress-strain curves from tensile test can be effectively used to quickly check and pick HEAs with superior SSS without computational-intensive theoretical models. In addition, it provides an opportunity to extract GB strengthening data concurrently instead of separate evaluation as is in the case of computational models. It is important to note that an increase in SSS does not guarantee a proportional improvement of the GB strengthening [39, 40].

2.1.4 Interstitial atoms

Interstitial atoms have successfully used in conventional alloys such as steels, to enhance by both SSS and precipitation of carbides and nitrides (as discussed in Section 2.4). Similarly, as illustrated in **Figure 2b**, carbon and nitrogen have been employed in HEAs to improve their mechanical properties. Stepanov et al. [52] investigated microstructure evolution and mechanical properties of CoCrFeNiMn-1(at.%)C after cold rolling and annealing between 800°C and 100°C. They established that the as-cast specimen had a fcc phase with a lattice parameter of 0.3595 nm, which is slightly higher than that of carbon-free CoCrFeMnNi (0.3593 nm) [53]. This increment of lattice parameter was attributed to the dissolved carbon. The friction stress of this alloy as obtained from the Hall-Petch relationship was reported to be 288.15 MPa, which is higher than 125 MPa reported by Otto et al. [12] for undoped CoCrFeMnNi. This increment of the lattice resistance to dislocation by more than two-fold can be attributed to the dissolved carbon, which induces lattice dilation of the crystal lattice as evidenced by an increase of the lattice parameter. This phenomenon is in agreement with the linear dependence of strength in stainless steels and TWIP steels, where 1 at.% of C induces 76.6 MPa and 42 MPa of strength, respectively. However, in CoCrFeMnNi HEA system, 1 at.% C induces approximately ~160 MPa of strength, indicating that carbon has a superior influence on the strength of HEAs than in steels [54]. In addition, a systematic addition of carbon up to 0.25 wt.% in CoCrFeMnNi HEA induced a proportional increase of lattice parameter from 0.3593 nm for undoped alloy to 0.3602 nm for the CoCrFeMnNi- $\text{C}_{0.25}$ in the as-solidified state [53]. Annealing heat treatment for between 600°C and 800°C of the as-solidified HEAs induces a decrease of the lattice parameter but increases again at 1000°C and 1200°C as shown in **Figure 8** below.

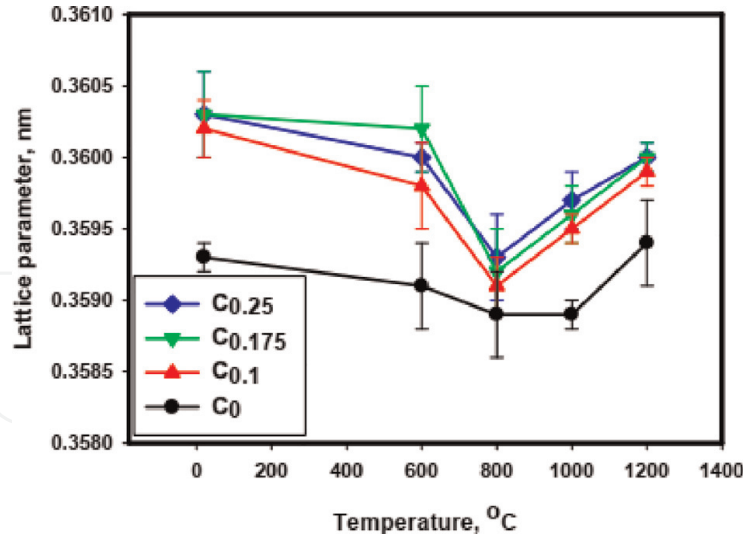


Figure 8. Dependence of lattice parameter of the CoCrFeNiMnCx ($x = 0; 0.1; 0.175; 0.25$) alloys on annealing temperature. Reprinted from Ref. [53].

3. Conclusion

It is evident that solid solution plays a critical role in the hardening of HEAs and the following conclusions can be inferred:

- i. The distortion of the crystal lattice strongly determines the degree of SSS in HEAs. And that the choice of elements has a great influence on the degree of lattice distortion which largely depends the atomic size of pure elements and the surrounding atom in HEAs. Based on the average interatomic spacing, it was Cr tends to enhance the strength of HEAs while Fe tends to have a softening effect as confirmed by both theoretical and experimental methods
- ii. HEAs with high residual mean strain tend to have a high intrinsic yield strength. The presence of some atoms such as Mn in CoCrFeMnNi HEA increases its strength by 14.3% compared to its quaternary subset CoCrFeNi because of the significant enhancement of the MSADs.
- iii. An integration of machine learning into alloy design provides a quicker pathway to screening a large compositional HEA space and identifying alloys with superior mechanical properties. For instance, it was predicted and verified experimentally using a modified ML-SSS model that non-equiatomic $\text{Fe}_{32}\text{Ni}_{12}\text{Cu}_{27}\text{Co}_{29}$ and $\text{Cr}_{18}\text{Mo}_{32}\text{Nb}_{35}\text{Ti}_{15}$ HEAs with FCC and BCC crystal structures, respectively, have higher hardness compared to their equiatomic counterparts.
- iv. In substitutional SS hardening, Al has been proven to be a strong SSS agent in fcc based HEAs. it is noteworthy that Al content more than ~ 11 at.% in $\text{Al}_x\text{CoCrFeNi}$ HEA system transforms the crystal structure from FCC to FCC + BCC and finally to fully BCC phase. This transformation is ascribed to the need for the FCC crystal structure to ‘shed off’ the excess energy from the distorted crystal lattice. Additionally, Nb has superior SSS ability both in FCC and BCC-based HEAs.

- v. Carbon can be used to improve the already available substitutional SSS in HEAs as it is the case in stainless steels. In fact, 1% C induces ~160 MPa of strength in equiatomic CoCrFeMnNi HEA compared to the 76.6 MPa in stainless steels and 42 MPa in TWIP steels.

Acknowledgements

The research was supported by the Kenyan German Centre for Mining, Environmental Engineering and Resource Management (CEMEREM) based at Taita Taveta University.

Author details

Ibrahim Ondicho^{1*}, Benard Alunda² and Kahinga Kamau³


1 Department of Mechanical Engineering, Dedan Kimathi University of Technology, Nyeri, Kenya

2 School of Mines and Engineering, Taita Taveta University, Voi, Kenya

3 Department of Chemistry, Jomo Kenyatta University of Agriculture and Technology, Nairobi, Kenya

*Address all correspondence to: ibrahim.ondicho@dkut.ac.ke

IntechOpen

© 2022 The Author(s). Licensee IntechOpen. This chapter is distributed under the terms of the Creative Commons Attribution License (<http://creativecommons.org/licenses/by/3.0>), which permits unrestricted use, distribution, and reproduction in any medium, provided the original work is properly cited. 

References

- [1] Kohyama A, Grossbeck ML, Piatti G. The application of austenitic stainless steels in advanced fusion systems: Current limitations and future prospects. *Journal of Nuclear Materials*. 1992;**191–194**(1992):37-44. DOI: 10.1016/S0022-3115(09)80008-1
- [2] Yeh JW. Recent progress in high-entropy alloys. *Annales de Chimie Science des Matériaux*. 2006;**31**(6): 633-648. DOI: 10.3166/acsm.31.633-648
- [3] Yeh JW. Alloy design strategies and future trends in high-entropy alloys. *JOM*. 2013;**65**(12):1759-1771. DOI: 10.1007/s11837-013-0761-6
- [4] Cantor B, Chang ITH, Knight P, Vincent AJB. Microstructural development in equiatomic multicomponent alloys. *Materials Science and Engineering A*. 2004;**375–377**:213-218. DOI: 10.1016/j.msea.2003.10.257
- [5] El-Atwani O et al. Outstanding radiation resistance of tungsten-based high-entropy alloys. *Science Advances*. 2019;**5**(3):eaav2002. DOI: 10.1126/sciadv.aav2002
- [6] He JY et al. A precipitation-hardened high-entropy alloy with outstanding tensile properties. *Acta Materialia*. 2016;**102**:187-196. DOI: 10.1016/j.actamat.2015.08.076
- [7] Tong Y et al. Outstanding tensile properties of a precipitation-strengthened FeCoNiCrTi0.2 high-entropy alloy at room and cryogenic temperatures. *Acta Materialia*. 2019;**165**: 228-240. DOI: 10.1016/j.actamat.2018.11.049
- [8] Xu S et al. Effect of oxygen content in 400 °C super-heated steam on the corrosion resistance of Zr-xSn-0.35Fe-0.15Cr-0.15 Nb alloys. *Corrosion Science*. 2022;**198**:110135. DOI: 10.1016/j.corsci.2022.110135
- [9] Wang Q et al. CoCrFeNiMo0.2 high entropy alloy by laser melting deposition: Prospective material for low temperature and corrosion resistant applications. *Intermetallics*. 2020;**119**:106727. DOI: 10.1016/j.intermet.2020.106727
- [10] Wu Y et al. Effect of high temperature molten salt corrosion on the microstructure of a Co-Mo-Cr-Si wear resistant alloy. *Materials Characterization*. 2021;**179**:111377. DOI: 10.1016/j.matchar.2021.111377
- [11] Shree Meenakshi K, Ananda Kumar S. Corrosion resistant behaviour of titanium – Molybdenum alloy in sulphuric acid environment. *Materials Today Proceedings*. 2022;**65**:3282-3287. DOI: 10.1016/j.matpr.2022.05.389
- [12] Otto F, Dlouhý A, Somsen C, Bei H, Eggeler G, George EP. The influences of temperature and microstructure on the tensile properties of a CoCrFeMnNi high-entropy alloy. *Acta Materialia*. 2013;**61**(15):5743-5755. DOI: 10.1016/j.actamat.2013.06.018
- [13] An XL et al. Hall-Petch relationship and corrosion behavior of cold-rolled CoNiFe medium entropy alloy. *Journal of Alloys and Compounds*. 2019;**807**:151698. DOI: 10.1016/j.jallcom.2019.151698
- [14] Liu WH et al. Ductile CoCrFeNiMo x high entropy alloys strengthened by hard intermetallic phases. *Acta Materialia*. 2016;**116**:332-342. DOI: 10.1016/j.actamat.2016.06.063
- [15] Li C, Li JC, Zhao M, Jiang Q. Effect of alloying elements on microstructure

and properties of multiprincipal elements high-entropy alloys. *Journal of Alloys and Compounds*. 2009;**475**: 752-757. DOI: 10.1016/j.jallcom.2008.07.124

[16] Wu Z, Parish CM, Bei H. Nano-twin mediated plasticity in carbon-containing FeNiCoCrMn high entropy alloys. *Journal of Alloys and Compounds*. 2015; **647**:815-822. DOI: 10.1016/j.jallcom.2015.05.224

[17] Li Z, Pradeep KG, Deng Y, Raabe D, Tasan CC. Metastable high-entropy dual-phase alloys overcome the strength-ductility trade-off. *Nature*. 2016; **534**(7606):227-230. DOI: 10.1038/nature17981

[18] Sabzi HE, Zarei Hanzaki A, Abedi HR, Soltani R, Mateo A, Roa JJ. The effects of bimodal grain size distributions on the work hardening behavior of a TRansformation-TWinning induced plasticity steel. *Materials Science and Engineering A*. 2016;**678**:23-32. DOI: 10.1016/j.msea.2016.09.085

[19] Sabzi HE et al. *Ab initio* assisted design of quinary dual-phase high-entropy alloys with transformation-induced plasticity. *Materials Science and Engineering A*. 2019;**636**:262-270. DOI: 10.1016/j.msea.2015.03.109

[20] Labusch R. A statistical theory of solid solution hardening. *Physica Status Solidi B: Basic Solid State Physics*. 1970; **41**(2):659-669. DOI: 10.1002/pssb.19700410221

[21] Fleischer RL. Substitutional solution hardening. *Acta Metallurgica*. 1963; **11**(3):203-209. DOI: 10.1016/0001-6160(63)90213-X

[22] Toda-Caraballo I, Rivera-Díaz-del-Castillo PEJ. Modelling solid solution

hardening in high entropy alloys. *Acta Materialia*. 2015;**85**:14-23. DOI: 10.1016/j.actamat.2014.11.014

[23] Gypen LA, Deruyttere A. Multi-component solid solution hardening. *Journal of Materials Science*. 1977;**12**(5): 1034-1038. DOI: 10.1007/BF00540988

[24] Okamoto NL, Yuge K, Tanaka K, Inui H, George EP. Atomic displacement in the CrMnFeCoNi high-entropy alloy – A scaling factor to predict solid solution strengthening. *AIP Advances*. 2016; **6**(12):125008. DOI: 10.1063/1.4971371

[25] Moon J et al. Mechanical behavior and solid solution strengthening model for face-centered cubic single crystalline and polycrystalline high-entropy alloys. *Intermetallics*. 2018;**98**:89-94. DOI: 10.1016/j.intermet.2018.04.022

[26] Ye YF, Liu CT, Yang Y. A geometric model for intrinsic residual strain and phase stability in high entropy alloys. *Acta Materialia*. 2015;**94**:152-161. DOI: 10.1016/j.actamat.2015.04.051

[27] Zhao YY, Nieh TG. Correlation between lattice distortion and friction stress in Ni-based equiatomic alloys. *Intermetallics*. 2017;**86**:45-50. DOI: 10.1016/j.intermet.2017.03.011

[28] Wu Z, Bei H, Pharr GM, George EP. Temperature dependence of the mechanical properties of equiatomic solid solution alloys with face-centered cubic crystal structures. *Acta Materialia*. 2014;**81**:428-441. DOI: 10.1016/j.actamat.2014.08.026

[29] Kako K, Kawakami E, Ohta J, Mayuzumi M. Effects of various alloying elements on tensile properties of high-purity Fe-18Cr-(14-16)Ni alloys at room temperature. *Materials Transactions*. 2002;**43**(2):155-162. DOI: 10.2320/matertrans.43.155

- [30] Van Drunen G, Saimoto S. The growth of Ni and Ni-Co single crystals. *Journal of Crystal Growth*. 1971;**11**(2):151-156. DOI: 10.1016/0022-0248(71)90179-5
- [31] Risal S, Zhu W, Guillen P, Sun L. Improving phase prediction accuracy for high entropy alloys with machine learning. *Computational Materials Science*. 2021;**192**:110389. DOI: 10.1016/j.commatsci.2021.110389
- [32] Zeng Y, Man M, Bai K, Zhang Y-W. Revealing high-fidelity phase selection rules for high entropy alloys: A combined CALPHAD and machine learning study. *Materials and Design*. 2021;**202**:109532. DOI: 10.1016/j.matdes.2021.109532
- [33] Li R, Xie L, Wang WY, Liaw PK, Zhang Y. High-throughput calculations for high-entropy alloys: A brief review. *Front. Mater.* 2020;**7**:290. DOI: 10.3389/fmats.2020.00290
- [34] Wen C et al. Modeling solid solution strengthening in high entropy alloys using machine learning. *Acta Materialia*. 2021;**212**:116917. DOI: 10.1016/j.actamat.2021.116917
- [35] Oh HS et al. Engineering atomic-level complexity in high-entropy and complex concentrated alloys. *Nature Communications*. 2019;**10**(1):Art. no. 1. DOI: 10.1038/s41467-019-10012-7
- [36] Huang X, Jin C, Zhang C, Zhang H, Fu H. Machine learning assisted modelling and design of solid solution hardened high entropy alloys. *Materials and Design*. 2021;**211**:110177. DOI: 10.1016/j.matdes.2021.110177
- [37] Ding Q et al. Tuning element distribution, structure and properties by composition in high-entropy alloys. *Nature*. 2019;**574**(7777):223-227. DOI: 10.1038/s41586-019-1617-1
- [38] Zhang F et al. Chemical complexity induced local structural distortion in NiCoFeMnCr high-entropy alloy. *Materials Research Letters*. 2018;**6**(8): 450-455. DOI: 10.1080/21663831.2018.1478332
- [39] Yoshida S, Ikeuchi T, Bhattacharjee T, Bai Y, Shibata A, Tsuji N. Effect of elemental combination on friction stress and Hall-Petch relationship in face-centered cubic high/medium entropy alloys. *Acta Materialia*. 2019;**171**:201-215. DOI: 10.1016/j.actamat.2019.04.017
- [40] Yoshida S, Bhattacharjee T, Bai Y, Tsuji N. Friction stress and Hall-Petch relationship in CoCrNi equi-atomic medium entropy alloy processed by severe plastic deformation and subsequent annealing. *Scripta Materialia*. 2017;**134**:33-36. DOI: 10.1016/j.scriptamat.2017.02.042
- [41] He Q, Yang Y. On lattice distortion in high entropy alloys. *Frontiers in Materials*. 2018;**5**:42. DOI: 10.3389/fmats.2018.00042
- [42] Tian F. A review of solid-solution models of high-entropy alloys based on *ab initio* calculations. *Frontiers in Materials*. 2017;**4**:36. DOI: 10.3389/fmats.2017.00036
- [43] Wang W-R, Wang W-L, Wang S-C, Tsai Y-C, Lai C-H, Yeh J-W. Effects of Al addition on the microstructure and mechanical property of Al_xCoCrFeNi high-entropy alloys. *Intermetallics*. 2012;**26**:44-51. DOI: 10.1016/j.intermet.2012.03.005
- [44] Chen H et al. Contribution of lattice distortion to solid solution strengthening in a series of refractory high entropy alloys. *Metallurgical and Materials Transactions A: Physical Metallurgy and Materials Science*. 2018;**49**(3):772-781. DOI: 10.1007/s11661-017-4386-1

- [45] Wang Z et al. Quantitative determination of the lattice constant in high entropy alloys. *Scripta Materialia*. 2019;**162**:468-471. DOI: 10.1016/j.scriptamat.2018.12.022
- [46] Nelson JB, Riley DP. An experimental investigation of extrapolation methods in the derivation of accurate unit-cell dimensions of crystals. *Proceedings of the Physical Society*. 1945;**57**(3):160-177. DOI: 10.1088/0959-5309/57/3/302
- [47] Agustianingrum MP, Yoshida S, Tsuji N, Park N. Effect of aluminum addition on solid solution strengthening in CoCrNi medium-entropy alloy. *Journal of Alloys and Compounds*. 2019;**781**:866-872. DOI: 10.1016/j.jallcom.2018.12.065
- [48] Hall EO. The deformation and ageing of mild steel: III discussion of results. *Proceedings of the Physical Society. Section B*. 1951;**64**(9):747-753. DOI: 10.1088/0370-1301/64/9/303
- [49] N. J. Petch. The Cleavage Strength of Polycrystals. 1953. Available from: <https://www.scinapse.io/papers/517706> [Accessed: May 25, 2021]
- [50] Sun SJ et al. Enhanced strength and ductility of bulk CoCrFeMnNi high entropy alloy having fully recrystallized ultrafine-grained structure. *Materials and Design*. 2017;**133**:122-127. DOI: 10.1016/j.matdes.2017.07.054
- [51] Ondicho I, Alunda B, Park N. Effect of Fe on the Hall-Petch relationship of (CoCrMnNi)_{100-x}Fe_x medium-and high-entropy alloys. *Intermetallics*. 2021;**136**:107239. DOI: 10.1016/j.intermet.2021.107239
- [52] Stepanov ND et al. Effect of thermomechanical processing on microstructure and mechanical properties of the carbon-containing CoCrFeNiMn high entropy alloy. *Journal of Alloys and Compounds*. 2017;**693**:394-405. DOI: 10.1016/j.jallcom.2016.09.208
- [53] Stepanov ND, Yurchenko NY, Tikhonovsky MA, Salishchev GA. Effect of carbon content and annealing on structure and hardness of the CoCrFeNiMn-based high entropy alloys. *Journal of Alloys and Compounds*. 2016;**687**:59-71. DOI: 10.1016/j.jallcom.2016.06.103
- [54] Bouaziz O, Zurob H, Chehab B, Embury JD, Allain S, Huang M. Effect of chemical composition on work hardening of Fe—Mn—C TWIP steels. *Materials Science and Technology*. 2011;**27**(3):707-709. DOI: 10.1179/026708309X12535382371852